ETH
Eidgenössische Technische Hochschule Zürich
Swiss Federal Institute of Technology Zurich

Seminar for Applied Mathematics SAM

Linearized Reconstruction for Diffuse Optical Spectroscopic Imaging

H. Ammari and B. Jin and W. Zhang

Research Report No. 2018-30
August 2018

Seminar für Angewandte Mathematik
Eidgenössische Technische Hochschule
CH-8092 Zürich
Switzerland

Linearized Reconstruction for Diffuse Optical Spectroscopic Imaging

Habib Ammari* Bangti Jin† Wenlong Zhang‡

Abstract

In this paper, we present a novel reconstruction method for diffuse optical spectroscopic imaging with a commonly used tissue model of optical absorption and scattering. It is based on linearization and group sparsity, which allows recovering the diffusion coefficient and absorption coefficient simultaneously, provided that their spectral profiles are incoherent and a sufficient number of wavelengths are judiciously taken for the measurements. We also discuss the reconstruction for imperfectly known boundary and show that with the multi-wavelength data, the method can reduce the influence of modelling errors and still recover the absorption coefficient. Extensive numerical experiments are presented to support our analysis.

Mathematics Subject Classification (MSC2000). 94A08, 35R30, 92C55.

Keywords. diffuse optical spectroscopic imaging, reconstruction algorithm, group sparsity, imperfectly known boundary.

1 Introduction

Diffuse optical spectroscopy (DOS) is a noninvasive and quantitative medical imaging modality, for reconstructing absorption and scattering properties from optical measurements at multiple wavelengths excited by the near-infrared (NIR) light. NIR light is particularly attractive for oncological applications because of its deep tissue penetrance and high sensitivity to haemoglobin concentration and oxygenation state [14]. DOS imaging effectively exploits the wavelength dependences of tissue optical properties (e.g. absorption, scattering, anisotropy, reduced scattering and refractive index), and such dependences have been measured and tabulated for various tissues [10, 21]. It was reported that the spectral dependence of tissue scattering contains much useful information for functional imaging [13, 28, 29]. For example, dual-wavelength spectroscopy has been widely used to determine the absorption coefficient and hence the concentrations of reduced hemoglobin and oxygenated hemoglobin in tissue [28]. Thus, DOS imaging holds significant potentials for many biomedical applications, e.g., breast oncology functional brain imaging, stroke monitoring, neonatal hymodynamics and imaging of breast tumours [12, 13, 14, 24].

In many biomedical applications, it is realistic to assume that the absorption coefficient is linked to the concentrations and the spectra of chromophores through a linear map (cf. (2.2) below), and the spectra of chromophores are known from experiments. Then the goal in DOS is to recover the individual concentrations from the measurements taken at multiple wavelengths. This task represents one of the most fundamental problems arising in accurate functional and molecular imaging. Theoretically, very little is known about uniqueness and stability of DOS (see [5, 6, 7] for related work in electrical impedance tomography (EIT) and [1, 3, 4, 9] for quantitative photoacoustic imaging).

*Department of Mathematics, ETH Zürich, Rämistrasse 101, CH-8092 Zürich, Switzerland (habib.ammari@math.ethz.ch).

†Department of Computer Science, University College London, London, WC1E 6BT, UK (b.jin@ucl.ac.uk,bangti.jin@gmail.com).

‡Department of Mathematics, Southern University of Science and Technology, 1088 Shenzhen, Guangdong, China (zhangwl@sustc.edu.cn).

Note that despite the linear dependence of absorption on the concentrations, the dependence of imaging data on the absorption coefficient is highly nonlinear. Further, it may suffer from severe ill-posedness and possible nonuniqueness; the latter is inherent to diffuse optical tomography of reconstructing simultaneously the absorption and diffusion coefficients [8]. Thus, the imaging problem is numerically very challenging. Nonetheless, there have been many important efforts in developing effective reconstruction algorithms using multi-wavelength data to obtain images and estimates of spatially varying concentrations of chromophores inside an optically scattering medium such as biological tissues. These include straightforward least-squares minimization [13], models-based minimization [23] and Bayesian approach [25]. Generally, there are two different ways to use the spectral measurements. One is to recover the optical parameters at each different wavelength separately and then fit the spectral parameter model to these optical parameters [9, 16, 26]; and the other is to express the optical parameters as a function of the spectral parameter model and then estimate the spectral parameter directly [23, 25, 31]. We refer the interested readers to the survey [15] and the references therein for detailed discussions.

In this paper, we shall develop a simple and efficient linearized reconstruction method for DOS to recover the absorption and diffusion coefficients. We employ the diffusion approximation to the radiative transfer equation for light transport, which has been used widely in biomedical optical imaging [8]. Our main contributions are as follows. First, we show that within the linearized regime, incoherent spectral dependence allows recovering the concentrations and diffusion coefficient simultaneously, provided that a sufficient number of measurements are judiciously taken. However, generally there is no explicit criterion on the number of wavelength, except in a few special cases (see Remark 1). Second, we demonstrate that with multi-wavelength measurements, the chromophore concentrations can be still be reasonably recovered even if the domain boundary is only imperfectly known. Thus, DOS can partially alleviate the deleterious effect of modeling errors, in a manner similar to multifrequency EIT [2]. Third and last, these analytical findings are verified by extensive numerical experiments, where the reconstruction is performed via a group sparse type recovery technique developed in [2].

The rest of the paper is organized as follows. In Section 2, we derive the linearized model, and discuss the conditions for simultaneous recovery (and also the one group sparse reconstruction technique). Then in Section 3, we demonstrate the potential of the multi-wavelength data for handling modeling errors, especially imperfectly known boundaries. We show that the chromophore concentrations can still be reasonably recovered from multi-wavelength data, but the diffusion coefficient is lost due to the corruption of domain deformation. Extensive numerical experiments are carried out in Section 4 to support the theoretical analysis. Finally, some concluding remarks are provided in Section 5.

2 The linearized diffuse optical spectroscopy model

In this section, we mathematically formulate the linearized multi-wavelength method in DOS.

2.1 Diffuse optical tomography

First, we introduce the diffuse optical tomography (DOT) model. Let $\Omega \subset \mathbb{R}^d$ $(d = 2, 3)$ be an open bounded domain with a smooth boundary $\partial\Omega$. The photon diffusion equation for the photon fluence rate u in the frequency domain takes the following form:

$$\begin{cases} -\nabla \cdot (D(x,\lambda)\nabla u) + \mu_a(x,\lambda)u = 0 & \text{in } \Omega, \\ D(x,\lambda)\dfrac{\partial u}{\partial \nu} + \alpha u = S & \text{on } \partial\Omega, \end{cases} \tag{2.1}$$

where ν is the unit outward normal vector to the boundary $\partial\Omega$, the nonnegative functions and D and μ_a denote the photon diffusion coefficient and absorption coefficient, respectively. In practice, the source function $S(x)$ is often taken to be a smooth approximation of the Dirac function δ_x at $x \in \partial\Omega$ [27]. The parameter α in the boundary condition is formulated as $\alpha = \frac{1-R}{2(1+R)}$ in DOT model, where R is a directionally varying refraction parameter [8]. The weak formulation of problem (2.1) is to find $u \in H^1(\Omega)$

such that

$$\int_\Omega D(x,\lambda)\nabla u\cdot\nabla v+\mu_a(x,\lambda)uv\mathrm{d}x+\int_{\partial\Omega}\alpha uv\mathrm{d}s=\int_{\partial\Omega}Sv\mathrm{d}s,\quad\forall v\in H^1(\Omega).$$

Here, $H^1(\Omega):=\{v\in L^2(\Omega):\nabla v\in L^2(\Omega)\}$.

In practice, the coefficients μ_a and D are actually depending on the light wavelength λ. The optical properties of the tissue can be expressed using their spectral representations. Commonly used spectral models for optical properties can be written as [9, 23, 26, 31]:

$$\mu_a(x,\lambda)=\sum_{k=1}^{K}\mu_k(x)s_k(\lambda), \tag{2.2}$$

$$\mu_s(x,\lambda)=\mu_{s,\mathrm{ref}}(\lambda/\lambda_{\mathrm{ref}})^{-b}, \tag{2.3}$$

where the absorption coefficient μ_a is expressed as chromophore concentrations μ_k weighted sum of K known chromophore absorption spectra s_k. The scattering coefficient μ_s is given, according to Mie scattering theory, as being proportional to $\mu_{s,\mathrm{ref}}$ and (scattering) power $-b$ of a relative wavelength $\lambda/\lambda_{\mathrm{ref}}$ [11, 18, 29]. The coefficient $\mu_{s,\mathrm{ref}}$ is known as the reduced scattering coefficient at a reference wavelength λ_{ref}, and it can be spatially dependent. In many types of tissues (e.g., muscle and skin tissues), the wavelength dependence of μ_s has been measured and can often be accurately approximated by $\mu_s(x,\lambda)=a(x)\lambda^{-b}$, where the exponent b is recovered from experiments [10, 21].

The optical diffusion coefficient $D(x,\lambda)$ is given by $D(x,\lambda)=[3(\mu_a+\mu_s)]^{-1}$. The condition $\mu_s\gg\mu_a$ is usually considered valid in order to ensure the accuracy of the diffusion approximation to the radiative transfer equation [15, 16, 8]. Hence, we assume below that the diffusion coefficient $D(x,\lambda)$ has the form:

$$D(x,\lambda)=d(x)s_0(\lambda), \tag{2.4}$$

where the wavelength dependence $s_0(\lambda)$ is known from experiments.

In DOT experiments, the tissue under consideration is illuminated with M sources, and measurements are taken at detectors. In this work, we assume for the sake of simplicity that the positions x_n of the sources and detectors are the same, and are distributed over the boundary $\partial\Omega$. The spectroscopic inverse problem is to recover the spatially-dependent coefficient $d(x)$ and the concentrations $\mu_k(x)$ of the chromophores given the measured data u (corresponding to the known sources S) on the detectors distributed on the boundary $\partial\Omega$ measured at several wavelengths λ_i. It is well-known that the inverse problem of recovering both coefficients $d(x)$ and $\mu_k(x)$ is quite ill-posed [16], since two different pairs of scattering and absorption coefficients can lead to identical measured data. The multi-wavelength method is a promising approach to resolve this challenging nonuniqueness issue. It is also reasonable to assume that the wavelength dependence $s_0(\lambda)$ and the absorption spectra $s_k(\lambda)$ are linearly independent so as to distinguish the diffusion coefficient and the chromophore concentrations by effectively using the information contained in the multi-wavelength data.

2.2 The linearized diffuse optical spectroscopy model

Now we derive the linearized DOS model, which plays a crucial role in the reconstruction technique. We discuss the cases of known and unknown diffusion coefficient separately.

2.2.1 Unknown diffusion coefficient

First, we derive the linearized model with both diffusion coefficient $D(x,\lambda)$ and concentrations $\mu_k(x)$ being unknown. For simplicity, we assume that the coefficient $d(x)$ is a small perturbation of the background, which is taken to be 1, i.e.,

$$d(x)=1+\delta d(x),$$

where the unknown perturbation $\delta d(x)$ has a compact support in the domain Ω and is small (in suitable $L^p(\Omega)$ norms).

For the inversion, smooth approximations S_n of the Dirac masses at $\{\delta_{x_n}\}_{n=1}^N$ are applied and the corresponding fluence rates u_n are measured on the detectors located at all x_n over the boundary $\partial\Omega$ to gain sufficient information about the diffusion coefficient $D(x,\lambda)$ and absorption coefficient $\mu_a(x,\lambda)$. That is, let $\{u_n \equiv u_n(x,\lambda)\}_{n=1}^N \subset H^1(\Omega)$ be the corresponding solutions to (2.1), i.e.,

$$\int_\Omega D(x,\lambda)\nabla u_n \cdot \nabla v + \mu_a(x,\lambda)u_n v \mathrm{d}x + \int_{\partial\Omega} \alpha u_n v \mathrm{d}s = \int_{\partial\Omega} S_n v \mathrm{d}s, \quad \forall v \in H^1(\Omega). \tag{2.5}$$

Next we derive the linearized multi-wavelength model for the DOT problem based on an integral representation. Let $v_m \equiv v_m(\lambda) \in H^1(\Omega)$ be the background solution corresponding to $D(\lambda,x) \equiv s_0(\lambda)$ and $\mu_a \equiv 0$ with the excitation S_m, i.e., v_m fulfils

$$\int_\Omega s_0(\lambda)\nabla v_m \cdot \nabla v \mathrm{d}x + \int_{\partial\Omega} \alpha v_m v \mathrm{d}s = \int_{\partial\Omega} S_m v \mathrm{d}s, \quad \forall v \in H^1(\Omega). \tag{2.6}$$

Note that unless $s_0(\lambda)$ is independent of the wavelength λ, the dependence of the background solution v_m on the wavelength λ cannot be factorized out. Taking $v = v_m$ in (2.5) and $v = u_n$ in (2.6) and subtracting the two identities yield

$$s_0(\lambda)\int_\Omega \delta d(x)\nabla u_n \cdot \nabla v_m \mathrm{d}x + \sum_{k=1}^K s_k(\lambda)\int_\Omega \mu_k(x) u_n v_m \mathrm{d}x = \int_{\partial\Omega} (S_n v_m - S_m u_n)\mathrm{d}s.$$

Since δd and μ_ks are assumed to be small, we can derive the approximations $\nabla u_n(x,\lambda) \approx \nabla v_n(x,\lambda)$ and $u_n(x,\lambda) \approx v_n(x,\lambda)$ in the domain Ω (valid in the linear regime), and hence arrive at the following linearized model

$$s_0(\lambda)\int_\Omega \delta d(x)\nabla v_n \cdot \nabla v_m \mathrm{d}x + \sum_{k=1}^K s_k(\lambda)\int_\Omega \mu_k(x) v_n v_m \mathrm{d}x = \int_{\partial\Omega} (S_n v_m - S_m u_n)\mathrm{d}s. \tag{2.7}$$

Note that since $\int_{\partial\Omega} S_m u_n \mathrm{d}s$ is the measured data on the detector located at x_m and $\int_{\partial\Omega} S_n v_m \mathrm{d}s$ can be computed given the background spectra $s_0(\lambda)$, the right-hand side of the model (2.7) is completely known.

The DOT imaging problem for the linearized model is to recover δd and the chromophores concentrations $\{\mu_k\}_{k=1}^K$ from $\{u_n(x,\lambda)\}_{n=1}^N$ on the boundary $\partial\Omega$ at several wavelengths $\{\lambda_q\}_{q=1}^Q$. For the reconstruction, we divide the domain Ω into a shape regular quasi-uniform mesh of elements $\{\Omega_l\}_{l=1}^L$ such that $\overline{\Omega} = \cup_{l=1}^L \Omega_l$, and consider a piecewise constant approximation of the coefficient $\delta d(x)$ and the concentrations $\{\mu_k\}_{k=1}^K$ of the chromophores as follows

$$\begin{aligned} \delta d(x) &\approx \sum_{l=1}^L (\delta d)_l \chi_{\Omega_l}(x), \\ \mu_k(x) &\approx \sum_{l=1}^L (\mu_k)_l \chi_{\Omega_l}(x), \quad k = 1,\ldots,K, \end{aligned}$$

where χ_{Ω_l} is the characteristic function of the lth element Ω_l, and $(\mu_k)_l$ denotes the value of the kth concentration $\delta\mu_k$ in the lth element Ω_l, so is $(\delta d)_l$. Upon substituting the approximation into (2.7), we have a finite-dimensional linear inverse problem

$$s_0(\lambda)\sum_{l=1}^L (\delta d)_l \int_{\Omega_l} \nabla v_n \cdot \nabla v_m \mathrm{d}x + \sum_{k=1}^K s_k(\lambda)\sum_{l=1}^L (\mu_k)_l \int_{\Omega_l} v_n v_m \mathrm{d}x = \int_{\partial\Omega} (S_n v_m - S_m u_n)\mathrm{d}s.$$

Finally, we introduce the sensitivity matrix $M^0(\lambda)$, $M^1(\lambda)$ and the data vector X. We use a single index $j = 1,\ldots,J$ with $J = N^2$ for the index pair (m,n) with $j = N(m-1)+n$, and introduce the

sensitivity matrix $M^0(\lambda) = [M^0_{jl}] \in \mathbb{R}^{J\times L}$ and $M^1(\lambda) = [M^1_{jl}] \in \mathbb{R}^{J\times L}$ with its entries M^1_{jl} given by

$$M^0_{jl}(\lambda) = \int_{\Omega_l} \nabla v_n \cdot \nabla v_m \mathrm{d}x \quad (j \leftrightarrow (m,n)),$$
$$M^1_{jl}(\lambda) = \int_{\Omega_l} v_n v_m \mathrm{d}x \quad (j \leftrightarrow (m,n)),$$

which is independent of the wavelength λ. Likewise, we introduce a data vector $X(\lambda) \in \mathbb{R}^J$ with its jth entry $X_j(\lambda)$ given by

$$X_j(\lambda) = \int_{\partial\Omega} (S_n v_m - S_m u_n)\mathrm{d}s \quad (j \leftrightarrow (m,n)).$$

By writing the vectors $A_0 = (\delta d)_l \in \mathbb{R}^L$ and $A_k = (\mu_k)_l \in \mathbb{R}^L$, $k = 0, \ldots, K$, we obtain the following linear system (parameterized by the light wavelength λ)

$$M^0(\lambda)s_0(\lambda)A_0 + M^1(\lambda)\sum_{k=0}^{K} s_k(\lambda)A_k = X(\lambda). \tag{2.8}$$

2.2.2 Known diffusion coefficient

If the diffusion coefficient $D(x,\lambda)$ is known, then the goal is to recover the concentrations $\{\mu_k\}_{k=1}^K$ of the chromophores. As before, we assume the unknowns μ_k are small (in suitable $L^p(\Omega)$ norms). We can repeat the above procedure, except that the background solution $v_m \in H^1(\Omega)$ is now defined by

$$\int_\Omega D(x,\lambda)\nabla v_m \cdot \nabla v \mathrm{d}x + \int_{\partial\Omega} \alpha v_m v \mathrm{d}s = \int_{\partial\Omega} S_m v \mathrm{d}s, \quad \forall v \in H^1(\Omega). \tag{2.9}$$

Taking $v = v_m$ in (2.5) and $v = u_n$ in (2.9) and subtracting the two identities gives

$$\sum_{k=1}^{K} s_k(\lambda) \int_\Omega \mu_k(x) u_n v_m \mathrm{d}x = \int_{\partial\Omega} (S_n v_m - S_m u_n)\mathrm{d}s.$$

Using the approximation $u_n(x,\lambda) \approx v_n(x,\lambda)$ in the domain Ω (which is valid in the linear regime), we arrive at the following linearized model

$$\sum_{k=1}^{K} s_k(\lambda) \int_\Omega \mu_k(x) v_n v_m \mathrm{d}x = \int_{\partial\Omega} (S_n v_m - S_m u_n)\mathrm{d}s.$$

As before, we divide the domain Ω into a shape regular quasi-uniform mesh of elements $\{\Omega_l\}_{l=1}^L$ such that $\overline{\Omega} = \cup_{l=1}^L \Omega_l$, and consider piecewise constant approximations of the chromophore concentrations μ_k:

$$\mu_k(x) \approx \sum_{l=1}^{L} (\mu_k)_l \chi_{\Omega_l}(x), \quad k = 1, \ldots, K.$$

Then we obtain the following finite-dimensional linear inverse problem

$$\sum_{k=1}^{K} s_k(\lambda) \sum_{l=1}^{L} (\mu_k)_l \int_{\Omega_l} v_n v_m \mathrm{d}x = \int_{\partial\Omega} (S_n v_m - S_m u_n)\mathrm{d}s.$$

Using the sensitivity matrix M and the data vector X in (2.8), we get the following parameterized linear system

$$M^1(\lambda)\sum_{k=1}^{K} s_k(\lambda)A_k = X(\lambda). \tag{2.10}$$

2.3 The linearized DOT with multi-wavelength data

In the two linearized DOT inverse problems in Section 2.2, the vectors A_0 (if $d(x)$ is unknown) and $\{A_k\}_{k=1}^K$ are the quantities of interest and are to be estimated from the wavelength dependent data $X(\lambda)$, given the spectra $s_0(\lambda)$ and $s_k(\lambda)$. These quantities directly contain the information of the locations and supports of $\delta d(x)$ and all the chromophores μ_k. Now we describe a procedure for recovering the coefficient $d(x)$ (if unknown) and the concentrations $\mu_k(x)$ of the chromophores simultaneously. The diffusion wavelength dependence $s_0(\lambda)$ is always known (e.g., $s_0(\lambda) = c\lambda^b$, where the parameter b is known from experiments [10]).

We first formulate the inversion method for the case an unknown diffusion coefficient $D(x)$. We consider the case when all the absorption coefficient spectra $\{s_k(\lambda)\}_{k=1}^K$ are known. Suppose that we have collated the measured data at Q distinct wavelengths $\{\lambda_q\}_{q=1}^Q$. We write $S = (s_k(\lambda_q)) \in \mathbb{R}^{K\times Q}$, $S_0 = (s_0(\lambda)) \in \mathbb{R}^{1\times Q}$. We also introduce the measured matrix $X = [X^t(\lambda_1) \ \dots \ X^t(\lambda_Q)]^t \in \mathbb{R}^{J\times Q,1}$ and the vector of unknowns $A = [A_1^t \ \dots \ A_K^t, A_0^t]^t \in \mathbb{R}^{L\times(K+1),1}$. Here, the superscript t denotes the matrix/vector transpose. Then we define a total sensitivity matrix M constructed by $Q\times(K+1)$ blocks. The (i,j)th block of M is $M^1(\lambda_i)s_j(\lambda_i)$ for $1 \le i \le Q$, $1 \le j \le K$ and the $(i,K+1)$th block of M is $M^1(\lambda_i)s_0(\lambda_i)$ for $1 \le i \le Q$. Hence, (2.8) yields the following linear system:

$$MA = X. \tag{2.11}$$

Similarly, when the diffusion coefficient $D(x,\lambda)$ is known, we define another total sensitivity matrix M constructed by $Q \times K$ blocks. The (i,j)th block of M is $M^1(\lambda_i)s_j(\lambda_i)$ for $1 \le i \le Q$, $1 \le j \le K$ and the vector of unknowns $A = [A_1^t \ \dots \ A_K^t]^t \in \mathbb{R}^{L\times K,1}$. We get from (2.10) the following linear system:

$$MA = X. \tag{2.12}$$

Remark 1. *Under the condition that the wavelength dependence of $M^0(\lambda)$ and $M^1(\lambda)$ can be factorized out (e.g., s_0 is independent of λ) (and thus can be absorbed into the spectra $s_k(\lambda)$), the linear systems can be decoupled to gain further insight. To see this, we consider the case* (2.11)*. Since all the spectra are assumed to be linearly independent, when a sufficient number of wavelengths $\{\lambda_q\}_{q=1}^Q$ are judiciously taken in the experiment, the corresponding spectral matrix $\tilde{S}^t = [S_0^t \ S^t]$ is incoherent in the sense that $Q \ge K+1$ and $\mathrm{rank}(S) = K+1$ and $\tilde{S}$ is also well-conditioned. Then the matrix $\tilde{S}$ has a right inverse $\tilde{S}^{-1}$. By letting $\tilde{Y} = X\tilde{S}^{-1}$, we obtain*

$$[M^0A_0, M^1A] = \tilde{Y}.$$

These are $K+1$ decoupled linear systems. By letting $\tilde{Y} = [\tilde{Y}_0 \ \dots \ \tilde{Y}_K] \in \mathbb{R}^{J\times(K+1)}$, we have $K+1$ independent (finite-dimensional) linear inverse problems

$$\begin{aligned} &M^0A_0 = \tilde{Y}_0, \\ &M^1A_k = \tilde{Y}_k, \quad k = 1,\dots,K, \end{aligned} \tag{2.13}$$

where A_0 represents the diffusion coefficient $\delta d(x)$ and A_k (for $1 \le k \le K$) represents the kth chromophore $\mu_k(x)$. Note that each linear system determines one and only one unknown concentration A_k. Similarly, for the case of a known diffusion coefficient, the matrix S has a right inverse S^{-1}, under the given incoherence assumption. By letting $Y = XS^{-1}$, we obtain

$$M^1A = Y.$$

These are K decoupled linear systems. By letting $Y = [Y_1 \ \dots \ Y_K] \in \mathbb{R}^{J\times(K+1)}$, we have K independent (finite-dimensional) linear inverse problems

$$M^1A_k = Y_k, \quad k = 1,\dots,K, \tag{2.14}$$

where A_k (for $1 \le k \le K$) represents the kth chromophore concentrations $\mu_k(x)$.

Below, we describe a group sparse reconstruction method developed in [2] to solve the ill-conditioned linear systems (2.11) and (2.12).

2.4 Group sparse reconstruction algorithm

Upon linearization and decoupling steps (see Remark 1), one arrives at decoupled linear systems of the form:

$$Dx = b, \tag{2.15}$$

where $D = M_0$ or $M \in \mathbb{R}^{J\times L}$ is the sensitivity matrix, $x = A_k \in \mathbb{R}^L$ $(0 \le k \le K)$ is the unknown vector, and $b = Y_k \in \mathbb{R}^J$ $(0 \le k \le K)$ is a known measured data. These linear systems are often under-determined, and severely ill-conditioned, due to the inherent ill-posed nature of the DOT inverse problem. We adapt a numerical sparse method developed in [2] to solve (2.15).

The algorithm takes the following two aspects into consideration:

(1) Under the assumption that the unknowns δd and μ_k are small, we may assume that x is sparse. This suggests to solve the minimization problem

$$\min_{x\in\Lambda} \|x\|_1 \quad \text{subject to } \|Dx - b\| \le \epsilon,$$

where $\|\cdot\|_1$ denotes the ℓ^1 norm of a vector. Here, Λ represents an admissible constraint on the unknowns x, since they are bounded from below and above, and $\epsilon > 0$ is an estimate of the noise level of b.

(2) In DOT applications, it is also reasonable to assume that each concentration of chromophore μ_k is clustered, and this refers to the concept of group sparsity. The grouping effect is useful to remove the undesirable spikes typically observed for the ℓ^1 penalty alone.

Now we describe the algorithm, i.e., group iterative soft thresholding, listed in Algorithm 1, adapted from iterative soft thresholding for ℓ^1 optimization [17]. Here, N is the maximum number of iterations, w_{lk} are nonnegative weights controlling the strength of interaction, and $\mathcal{N}_l$ denotes the neighborhood of the lth element. We take $w_{lk} = \beta$, for some $\beta > 0$ (default: $\beta = 0.5$), and $\mathcal{N}_l$ consists of all elements in the triangulation sharing one edge with the lth element. Since the solution x is expected to be sparse, a natural choice of the initial guess x^0 is the zero vector. The regularization parameter γ plays a crucial role in the performance of the reconstruction quality: the larger the value γ is, the sparser the reconstructed solution becomes. There are several possible strategies to determine its value, e.g., discrepancy principle and balancing principle, or a trial-and-error manner [20].

Below we briefly comment on the main steps of the algorithm and refer to [2] for details.

Step 3 g^j is a gradient descent update of x^j, and $s^j > 0$ is the step length, e.g., $s^j = 1/\|D\|^2$.

Step 4 This step takes into account the neighboring influence.

Step 5 $\bar{d}^j$ indicates a grouping effect: the larger $\bar{d}^j_l$ is, the more likely the lth element belongs to the group.

Step 6 This step rescales γ to be inversely proportional to $\bar{d}^j_l$.

Step 7 This step performs the projected thresholding with a spatially variable $\bar{\alpha}^j$. P_Λ denotes the pointwise projection onto the constraint set Λ and S_λ for $\lambda > 0$ is defined by $S_\lambda(t) = \max(|t| - \lambda, 0)\,\mathrm{sign}(t)$.

In our numerical experiments, we apply Algorithm 1 to the coupled linear systems (2.11) and (2.12) directly. This can be achieved by a simple change to Algorithm 1. Specifically, at Step 3 of the algorithm, instead we compute the gradient of the least-squares functional $\frac{1}{2}\|MA - Y\|^2$ by

$$g^j = A^j - s^j M^t(Mx^j - Y).$$

The remaining steps of the algorithm are applied to each component A_i independently. Note that one can easily incorporate separately a regularization parameter γ on each component, which is useful since the diffusion and scattering coefficients are likely to have different magnitudes.

Algorithm 1 Group iterative soft thresholding.

1: Input D, b, W, $\mathcal{N}$, γ, N and x^0;
2: **for** $j = 1, \ldots, N$ **do**
3: Compute the proxy g^j by

$$g^j = x^j - s^j D^t(Dx^j - b);$$

4: Compute the generalized proxy d^j by

$$d_l^j = |g_l^j|^2 + \sum_{k \in \mathcal{N}_l} w_{lk} |g_k^j|^2;$$

5: Compute the normalized proxy $\bar{d}^j$ by

$$\bar{d}^j = \max(d^j)^{-1} d^j;$$

6: Adapt the regularization parameter $\bar{\alpha}^j$ by

$$\bar{\alpha}_l^j = \gamma / \bar{d}_l^j, \quad l = 1, \ldots, L;$$

7: Update x^{j+1} by the group thresholding

$$x^{j+1} = P_\Lambda(S_{s^j \bar{\alpha}^j}(g^j));$$

8: Check the stopping criterion.
9: **end for**

3 Imperfectly known boundary

Now, in order to show the potentials of DOS for handling modelling errors, we consider the case where the boundary of the domain of interest is not perfectly known. This is one type of the modelling errors that occurs whenever the positions of the point sources and detectors or the domain of interest are not perfectly modelled.

We denote the true but unknown physical domain by $\widetilde{\Omega}$, and the computational domain by Ω, which approximates $\widetilde{\Omega}$. Next, we introduce a forward map $F : \widetilde{\Omega} \to \Omega$, $\widetilde{x} \to x$, which is assumed to be a smooth orientation-preserving map with a sufficiently smooth inverse map $F^{-1} : \Omega \to \widetilde{\Omega}$. We denote the Jacobian of the map F by J_F, and the Jacobian of F with respect to the surface integral by J_F^S.

Suppose now that the function $\widetilde{u}_n(\widetilde{x}, \lambda)$ satisfies problem (2.1) in the true domain $\widetilde{\Omega}$ with the diffusion coefficient $\widetilde{D}(\widetilde{x}, \lambda)$, absorption coefficient $\widetilde{\mu}_a(\widetilde{x}, \lambda)$ and source $\widetilde{S}(\widetilde{x})$, namely

$$\begin{cases} -\nabla_{\widetilde{x}} \cdot (\widetilde{D}(\widetilde{x}, \lambda) \nabla_{\widetilde{x}} \widetilde{u}_n(\widetilde{x}, \lambda)) + \widetilde{\mu}_a(\widetilde{x}, \lambda) \widetilde{u}_n = 0 & \text{in } \widetilde{\Omega}, \\ \widetilde{D}(\widetilde{x}, \lambda) \dfrac{\partial \widetilde{u}_n}{\partial \widetilde{\nu}}(\widetilde{x}) + \alpha \widetilde{u}_n(\widetilde{x}) = \widetilde{S}_n(\widetilde{x}) & \text{on } \partial\widetilde{\Omega}. \end{cases} \tag{3.1}$$

Here, $\widetilde{S}_n$ is a smooth approximation of the Dirac mass at the true position $\widetilde{x}_n$. The wavelength-dependent absorption coefficient $\widetilde{\mu}(\widetilde{x}, \lambda)$ also has a separable form related to the true concentrations $\widetilde{\mu}_k(\widetilde{x})$ of the chromophres:

$$\widetilde{\mu}_a(\widetilde{x}, \lambda) = \sum_{k=1}^{K} \widetilde{\mu}_k(\widetilde{x}) s_k(\lambda), \tag{3.2}$$

where $\widetilde{\mu}_k$ are assumed to be small. Furthermore, the diffusion coefficient D takes the linear form:

$$\widetilde{D}(\widetilde{x}, \lambda) = s_0(\lambda)(1 + \widetilde{\delta d}(\widetilde{x})). \tag{3.3}$$

The weak formulation of problem (3.1) is given by: find $\widetilde{u}_n(\cdot,\lambda) \in H^1(\widetilde{\Omega})$ such that

$$\int_{\widetilde{\Omega}} \widetilde{D}(\widetilde{x},\lambda)\nabla_{\widetilde{x}}\widetilde{u}_n \cdot \nabla_{\widetilde{x}}\widetilde{v} + \widetilde{\mu}_a(\widetilde{x},\lambda)\widetilde{u}_n\widetilde{v}\mathrm{d}\widetilde{x} + \int_{\partial\widetilde{\Omega}} \alpha\widetilde{u}_n\widetilde{v}\mathrm{d}\widetilde{s} = \int_{\widetilde{\Omega}} \widetilde{S}_n\widetilde{v}\mathrm{d}\widetilde{s}, \quad \forall\widetilde{v} \in H^1(\widetilde{\Omega}). \tag{3.4}$$

In the experimental settings, $\widetilde{u}_n$ is assumed to be measured on the boundary $\partial\widetilde{\Omega}$. However, because of the incorrect knowledge of $\partial\widetilde{\Omega}$, the measured quantity is in fact $u_n := \widetilde{u}_n \circ F^{-1}$ restricted to the computational boundary $\partial\Omega$. Below we consider only the case that the domain Ω is a small variation of the true physical one $\widetilde{\Omega}$, so that the linearized regime is valid. Specifically, the map $F : \widetilde{\Omega} \to \Omega$ is given by $F(\widetilde{x}) = \widetilde{x} + \epsilon\widetilde{\phi}(\widetilde{x})$, where ϵ is a small scalar and the smooth function $\widetilde{\phi}(\widetilde{x})$ characterizes the domain deformation. Further, let $F^{-1}(x) = x + \epsilon\phi(x)$ be the inverse map, which is also smooth.

In order to analyze the influence of the domain deformation on the linearized DOT problem, we introduce the solution $v_m \in H^1(\Omega)$ corresponding to $\bar{D}(\lambda,x) \equiv s_0(\lambda)$ and $\mu_a \equiv 0$ with S_m being a smooth approximation of δ_{x_m}, i.e., v_m fulfils

$$\int_\Omega s_0(\lambda)\nabla v_m \cdot \nabla v\mathrm{d}x + \int_{\partial\Omega} \alpha v_m v\mathrm{d}s = \int_{\partial\Omega} S_m v\mathrm{d}s, \qquad v \in H^1(\Omega). \tag{3.5}$$

Now we can state the corresponding linearized DOT problem with an unknown boundary. The result indicates that even for an isotropic diffusion coefficient $\widetilde{D}$ in the true domain $\widetilde{\Omega}$, in the computational domain Ω the equivalent diffusion coefficient D is generally anisotropic, and there is an additional perturbation factor on the boundary $\partial\Omega$.

Proposition 3.1. *Let $\mu_a = \widetilde{\mu}_a \circ F^{-1}$. The linearized inverse problem on the domain Ω is given by*

$$\begin{aligned} s_0(\lambda)\left(\int_\Omega (\delta d(x) + \epsilon\Psi)\nabla v_n \cdot \nabla v_m\mathrm{d}x\right) + \int_{\partial\Omega} \alpha\epsilon\psi v_n v_m\mathrm{d}s + \sum_{k=1}^K s_k(\lambda)\int_\Omega \mu_k(x)v_n v_m\mathrm{d}x \\ = \int_{\partial\Omega} (S_n v_m - S_m u_n)\mathrm{d}s, \end{aligned} \tag{3.6}$$

for some smooth functions $\Psi : \Omega \to \mathbb{R}^{d\times d}$ and $\psi : \partial\Omega \to \mathbb{R}$, which are independent of the wavelength λ.

Proof. First, we derive the governing equation for the variable $u_n = \widetilde{u}_n \circ F^{-1}$ in the domain Ω from (3.4). Let $v = \widetilde{v} \circ F^{-1} \in H^1(\Omega)$. By the chain rule, we have $\nabla_{\widetilde{x}}\widetilde{u}_n \circ F^{-1} = (J_F^t \circ F^{-1})\nabla_x u_n$, where the superscript t denotes the matrix transpose. Thus, we deduce that

$$\begin{aligned} &\int_{\widetilde{\Omega}} \widetilde{D}(\widetilde{x},\lambda)\nabla_{\widetilde{x}}\widetilde{u}_n(\widetilde{x})\cdot\nabla_{\widetilde{x}}\widetilde{v}(\widetilde{x})\mathrm{d}\widetilde{x} \\ &= \int_\Omega (\widetilde{D} \circ F^{-1})(x)(J_F^t \circ F^{-1})(x)\nabla u_n(x) \cdot (J_F^t \circ F^{-1})(x)\nabla v(x)|\det J_F(x)|^{-1}\mathrm{d}x \\ &= \int_\Omega (J_F \circ F^{-1})(x)(\widetilde{D} \circ F^{-1})(x)(J_F^t \circ F^{-1})(x)\nabla u_n(x) \cdot \nabla v(x)|\det J_F(x)|^{-1}\mathrm{d}x \\ &= \int_\Omega D(x,\lambda)\nabla u_n(x) \cdot \nabla v(x)\,\mathrm{d}x, \end{aligned}$$

where the transformed diffusion coefficient $D(x,\lambda)$ is given by [30, 22, 2]

$$D(x,\lambda) = \left(\frac{J_F(\cdot)\widetilde{D}(\cdot,\lambda)J_F^t(\cdot)}{|\det J_F(\cdot)|} \circ F^{-1}\right)(x).$$

Similarly, we obtain

$$\begin{aligned} \int_{\widetilde{\Omega}} \widetilde{\mu}_a(\widetilde{x},\lambda)\widetilde{u}_n(\widetilde{x})\widetilde{v}(\widetilde{x})\mathrm{d}\widetilde{x} &= \int_\Omega \mu_a(x,\lambda)u_n(x)v(x)|\det J_F(x)|^{-1}\,\mathrm{d}x, \\ \int_{\partial\Omega} \alpha\widetilde{u}_n\widetilde{v}\mathrm{d}\widetilde{s} &= \int_{\partial\Omega} \alpha u_n v|\det J_F^S(x)|^{-1}\mathrm{d}s. \end{aligned}$$

Here we use the fact that $\widetilde{D} \equiv 1$ near the boundary in the second equation, since δd is compactly supported in the domain. From (3.4), it follows that u_n satisfies

$$\int_\Omega D(x,\lambda)\nabla u_n \cdot \nabla v + \mu_a(x,\lambda)u_n v|\det J_F(x)|^{-1}\mathrm{d}x + \int_{\partial\Omega} \alpha u_n v|\det J_F^S(x)|^{-1}\mathrm{d}s = \int_{\partial\Omega} S_n v \mathrm{d}s, \quad \forall v \in H^1(\Omega). \tag{3.7}$$

Then by choosing $v = v_m$ in (3.7) and $v = u_n$ in (3.5), we arrive at

$$\int_\Omega (D(x,\lambda) - s_0(\lambda))\nabla v_n \cdot \nabla v_m \mathrm{d}x + \int_\Omega \mu_a(x) v_n v_m |\det J_F(x)|^{-1}\mathrm{d}x + \int_{\partial\Omega} \alpha(|\det J_F^S(x)|^{-1} - 1)u_n v \mathrm{d}s = \int_{\partial\Omega} (S_n v_m - S_m u_n)\mathrm{d}s. \tag{3.8}$$

Note that $J_F = I + \epsilon J_{\widetilde{\phi}}$, and $J_{F^{-1}} = I + \epsilon J_\phi = I - \epsilon J_{\widetilde{\phi}} \circ F^{-1} + O(\epsilon^2)$, since ϵ is small. It is known that $|\det J_F| = 1 - \epsilon \mathrm{div}\widetilde{\phi} + O(\epsilon^2)$ [19, equation (2.10)], we similarly derive $|\det J_F^S| = 1 + \epsilon\psi + O(\epsilon^2)$. Then $D(x,\lambda)$ is given by

$$\begin{aligned} D(x,\lambda) &= \widetilde{D}(\cdot,\lambda)(1 + \epsilon \mathrm{div}\widetilde{\phi}(\cdot))^{-1}(I + \epsilon(J_{\widetilde{\phi}}(\cdot) + J_{\widetilde{\phi}}^t(\cdot))) \circ F^{-1}(x) + O(\epsilon^2) \\ &= \widetilde{D}(\cdot,\lambda)((1 - \epsilon \mathrm{div}\widetilde{\phi}(\cdot))I + \epsilon(J_{\widetilde{\phi}}(\cdot) + J_{\widetilde{\phi}}^t(\cdot))) \circ F^{-1}(x) + O(\epsilon^2) \\ &= \widetilde{D}(\cdot,\lambda)(1 + \Psi\epsilon) \circ F^{-1}(x) + O(\epsilon^2), \end{aligned}$$

where $\Psi = (J_{\widetilde{\phi}} + J_{\widetilde{\phi}}^t - \mathrm{div}\widetilde{\phi} I)$ is smooth and independent of λ. This and the linear form of $\widetilde{\mu}_a(\widetilde{x},\lambda)$ in (3.3) yield

$$D(x,\lambda) \approx s_0(\lambda)I + \epsilon s_0(\lambda)\Psi(x) \quad \text{and} \quad \mu_a(x)|\det J_F(x)|^{-1} = \sum_{k=1}^K \mu_k(x)s_k(\lambda) + o(\epsilon),$$

where we have used the assumption that the μ_k are small. Upon substituting the above expressions into (3.8) and the approximations $\nabla u_n \approx \nabla v_n$, $u_n \approx v_n$ in the domain, we obtain (3.6). □

By Proposition 3.1, in the presence of an imperfectly known boundary with its magnitude ϵ being comparable with the concentrations $\{\mu_k\}_{k=1}^K$ and the perturbation δd, the perturbed sensitivity system contains significantly modeling errors resulting from the domain deformation. Thus, a direct inversion of the linearized model (3.6) is unsuitable. This issue can be resolved using the multi-wavelength approach as follows. Since (3.6) is completely analogous to (2.7), with the only difference lying in the additional terms in $s_0(\lambda)$ (corresponding to the diffusion coefficient) and the edge perturbation $\int_{\partial\Omega} \alpha\epsilon\psi v_n v_m \mathrm{d}s$. However, the edge perturbation on the boundary $\partial\Omega$ can be treated as unknowns corresponding to an additional spectral profile $s_*(\lambda) \equiv 1$.

Now assume that the spectral profiles $s_0, s_1, ..., s_K$, and s_* are incoherent. Hence, the method in Section 2.2 may be applied straightforwardly, since the right-hand side is known. However, the diffusion perturbation δd will never be properly reconstructed, due to the pollution of the error term $\epsilon\Psi$. The concentration of chromophores μ_k corresponding to the wavelength spectrum s_k, $k = 1, \ldots, K$ may be reconstructed, since they are affected by the deformation only through $\mu_k = \widetilde{\mu}_k \circ F^{-1}$. That is, the location and shape can be slightly deformed. Only the information of the diffusion coefficient is affected, and cannot be reconstructed. In summary, multi-wavelength DOT is very effective to eliminate the modelling errors caused by the boundary uncertainty, at least in the linearized regime.

We have discussed that the influence of an uncertain boundary in the case where both diffusion and absorption coefficients are unknown. We can also analyze for the case with a known diffusion coefficient similarly. Specifically, one may assume the deformed diffusion coefficient on the domain $\bar{D}(x,\lambda) = \widetilde{D}(\widetilde{x},\lambda) \circ F^{-1}$ and repeat the procedure of Proposition 3.1. We just give the conclusion: when the diffusion coefficient is known, the domain deformation contributes to a perturbation inside the spectrum s_0, and the boundary deformation pollutes the known diffusion term, and the concentration of chromophores μ_k corresponding to the wavelength spectrum s_k, $k = 1, \ldots, K$ could be reconstructed.

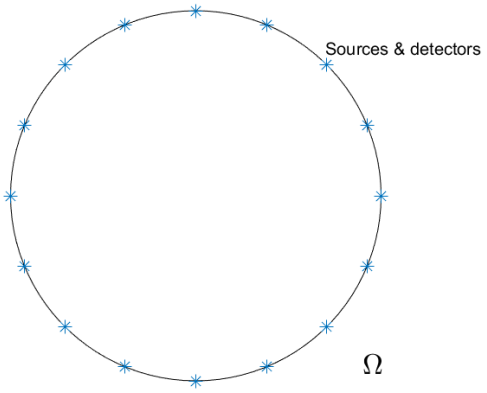

Figure 4.1: The true boundary shape, the positions of sources and detectors.

4 Numerical experiments

Now we show some numerical results to illustrate our analytical findings. The general setting for the numerical experiments is as follows. The domain Ω is taken to be the unit circle $\Omega = \{(x_1, x_2) : x_1^2 + x_2^2 < 1\}$. There are 16 point sources uniformly distributed along the boundary $\partial\Omega$; see Figure 4.1 for a schematic illustration of the domain Ω, the point sources and the detectors.

Furthermore, we assume that the spectral profile $s_0(\lambda)$ for the diffusion coefficient is $s_0(\lambda) = 0.2\lambda^b$, where the parameter b is known from experiments [10]. In all the examples below, we take $b = 1.5$. We will also see that $\mu_s \gg \mu_a$ is fulfilled in all the numerical examples. We take a directionally varying refraction parameter $R = 0.2$, so that $\alpha = \frac{1-R}{2(1+R)} = 1/3$. We use a piecewise linear finite element method on a shape regular quasi-uniform triangulation of the domain Ω. The unknowns are represented on a coarser finite element mesh using a piecewise constant finite element basis. We measure the data $u_n(x_m, \lambda)(:= \int_{\partial\Omega} S_m u_n \mathrm{d}s)$ on the detectors located at x_m. The noisy data $u_n^\delta(x_m, \lambda)$ is generated by adding Gaussian noise to the exact data $u_n^\dagger(x_m, \lambda)$ corresponding to the true diffusion coefficient $D(x, \lambda)$ and absorption coefficient $\mu_a(x, \lambda)$ by

$$u_n^\delta(x_m, \lambda) = u_n^\dagger(x_m, \lambda) + \eta \max_l |u_n^\dagger(x_m, \lambda) - v_n(x_m, \lambda)| \xi_{n,m},$$

where η is the noise level, and $\xi_{n,m}$ follows the standard normal distribution.

We present the numerical results for the cases with known boundary and with imperfectly known boundary separately, and for each case, we also present the examples with the diffusion coefficient being known and unknown. In Algorithm 1, we take a constant step size to solve (2.15).

4.1 Perfectly known boundary

First, we show numerical results for the case with a perfectly known boundary shape. We shall test the robustness of the algorithm against the noise, and show that the multi-wavelength approach could reduce the deleterious effects of the noise in the measured data. The regularization parameter γ was determined by a trial-and-error manner, and it was fixed at $\gamma = 5 \times 10^{-3}$ for the diffusion coefficient and $\gamma = 1 \times 10^{-4}$ for the absorption coefficient in all the numerical examples with perfectly known boundary. This algorithm is always initialized with a zero vector.

Example 4.1. *Consider a known diffusion coefficient $D(\lambda, x) = s_0(\lambda) = 0.2\lambda^{1.5}$, and two chromophores inside the domain: the wavelength dependence of the chromophore on the top is $s_1(\lambda) = 0.2\lambda$, and the one on the bottom is $s_2(\lambda) = 0.2(\lambda - 1)^2$; See Figure 4.2 for an illustration. We take measurements at $Q = 3$ wavelengths with $\lambda_1 = 1$, $\lambda_2 = 1.5$ and $\lambda_3 = 2$.*

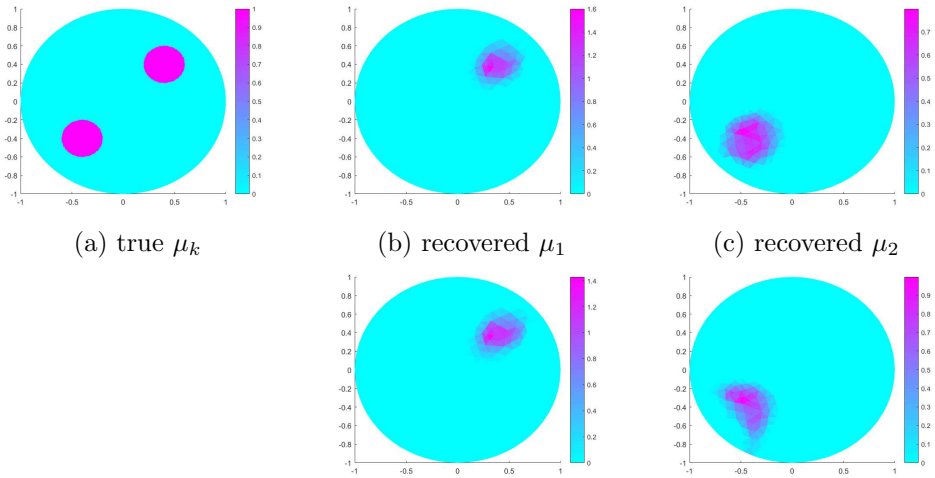

(a) true μ_k (b) recovered μ_1 (c) recovered μ_2

(d) recovered μ_1 (e) recovered μ_2

Figure 4.2: Numerical results for Example 4.1: (a) exact μ_1 and μ_2 of two chromophores; (b)–(c) recovered results with $\eta = 1\%$ noise level; (d)–(e) recovered results with $\eta = 10\%$ noise level.

The numerical results for Example 4.1 are presented in Figure 4.2. It is observed that the recovery is very localized within a clean background even with 10% noise in the data, and the supports of the recovered concentrations of the chromophores agree closely with the true ones and the magnitudes are well-retrieved. Remarkably, the increase of the noise level from 1% to 10% does not influence much the shape of the recovered concentrations. Therefore, if the given spectral profiles $s_k(\lambda)$ are sufficiently incoherent, the corresponding unknowns can be fairly recovered. This example also show that the proposed multi-wavelength approach is very robust to data noise, due to strong prior imposed by the group sparsity approach.

The next example shows the approach for reconstructing three chromophores inside the domain.

Example 4.2. *Consider the case with a known diffusion coefficient* $D(\lambda, x) = s_0(\lambda) = 0.2\lambda^{1.5}$*, and 3 chromophores inside the domain:*

(i) The two chromophores on the top share the wavelength dependence $s_1(\lambda) = 0.2\lambda$*, and the one on the bottom has a second spectral profile* $s_2(\lambda) = 0.2(\lambda - 1)^2$*;*

(ii) The wavelength dependence of the chromophore on the top right is $s_1(\lambda) = 0.2(\lambda - 1)^2$*, of the top left one is* $s_2(\lambda) = 0.2\lambda$ *and of the bottom is* $s_3(\lambda) = 0.2(\lambda - 1)^3$*.*

We take measurements at $Q = 3$ *wavelengths with* $\lambda_1 = 1$*,* $\lambda_2 = 1.5$ *and* $\lambda_3 = 2$ *and the noise level is set to be* $\eta = 1\%$*.*

The reconstruction results for Example 4.2 are shown in Figure 4.3. Figure 4.3 indicates that the unknowns corresponding to two or three spectral profiles can be fairly recovered in terms of both the supports and magnitudes. In case (i), the two chromophores on the top share the wavelength dependence, and they are recovered simultaneously; whereas in case (ii), the chromophores have three incoherent wavelength dependences, and they can be recovered separately.

The next example aims at recovering both diffusion and absorption coefficients, which is known to be very challenging in the absence of multi-wavelength data.

Example 4.3. *Consider the case of an unknown diffusion coefficient given by* $D(\lambda, x) = s_0(\lambda)(1 + 0.1\delta d(x)) = 0.2\lambda^{1.5}(1+0.25\delta d(x))$*. Similar to Example 4.1, consider two chromophores inside the domain: the wavelength dependence of the chromophore on the top is* $s_1(\lambda) = 0.2\lambda$*, and that of the bottom is*

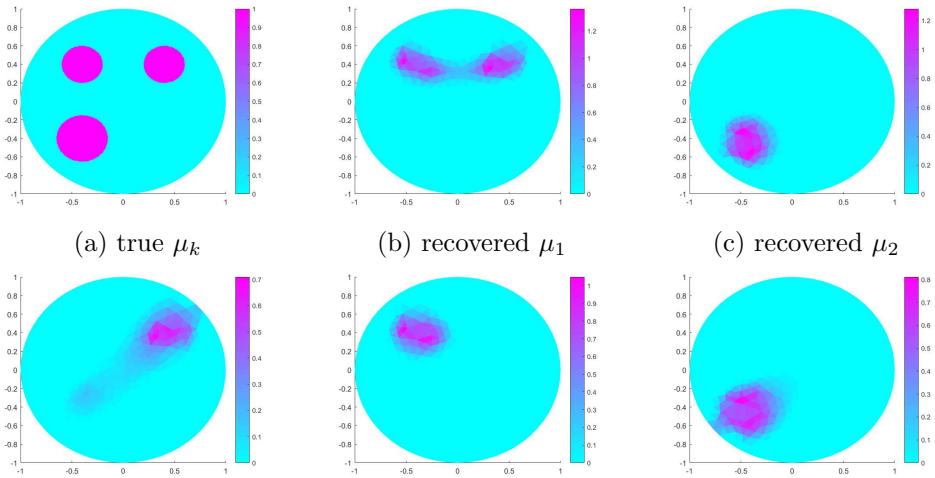

(a) true μ_k (b) recovered μ_1 (c) recovered μ_2

(d) recovered μ_1 (e) recovered μ_2 (f) recovered μ_3

Figure 4.3: Numerical results for Example 4.2: (a) exact μ_1 and μ_2 of two chromophores; (b)-(c) recovered results for case (i) (noise level $\eta = 1\%$); (d)-(f) recovered results for case (ii) (noise level $\eta = 1\%$).

$s_2(\lambda) = 0.2(\lambda - 1)^2$. *The measurements are taken at* $Q = 3$ *wavelengths with* $\lambda_1 = 1$, $\lambda_2 = 1.5$ *and* $\lambda_3 = 2$, *and the noise level* η *is fixed at* $\eta = 1\%$.

The numerical results for Example 4.3 are shown in Figure 4.4. Simultaneously reconstructing the diffusion and absorption coefficients is more sensitive to data noise, when compared with the case of a known diffusion coefficient. Recall that the problem of recovering both coefficients is quite ill-posed [16]: two different pairs of scattering and absorption coefficients can give rise to identical measured data. However, it is observed from Example 4.3 that the multi-wavelength approach allows overcoming this nonuniqueness issue, provided that the spectra are indeed incoherent.

The next example shows that multi-wavelength data can mitigate the effects of the noise.

Example 4.4. *Consider the setting of Example 4.3, but with a noise level* $\eta = 30\%$. *We study two different numbers of wavelengths.*

(i) The measurements are taken at $Q = 3$ *wavelengths with* $\lambda_i = 1 + (i-1)/2$, $i = 1, \ldots, 3$;

(ii) The measurements are taken at $Q = 30$ *wavelengths with* $\lambda_i = 1 + (i-1)/29$, $i = 1, \ldots, 30$.

Numerical results for Example 4.4 are shown in Figure 4.5. When using only data for 3 wavelengths, the recovered images are blurred by 30% noise. However, using data for 30 wavelengths, both the diffusion coefficient δd and two chromophore concentrations μ_k are much better resolved than using data with 3 wavelengths. Hence, more wavelength observations can greatly mitigate the effects of data noise; which concurs with the observations from the experimental study [29].

4.2 Imperfectly known boundary

Now we illustrate the approach in the case of an imperfectly known boundary. The (unknown) true domain $\widetilde{\Omega}$ is an ellipse centered at the origin with semi-axes a and b, $\mathcal{E}_{a,b} = \{(x_1, x_2) : x_1^2/a^2 + x_2^2/b^2 < 1\}$, and the computational domain Ω is the unit disk. In this part, the regularization parameter γ was determined by a trial-and-error manner, and it was fixed at $\gamma = 5 \times 1^{-2}$ for the diffusion coefficient, $\gamma = 1 \times 10^{-4}$ for the absorption coefficient and $\gamma = 1 \times 10^{-4}$ for the edge perturbation in all the numerical examples with imperfectly known boundary. This algorithm is always initialized with a zero vector.

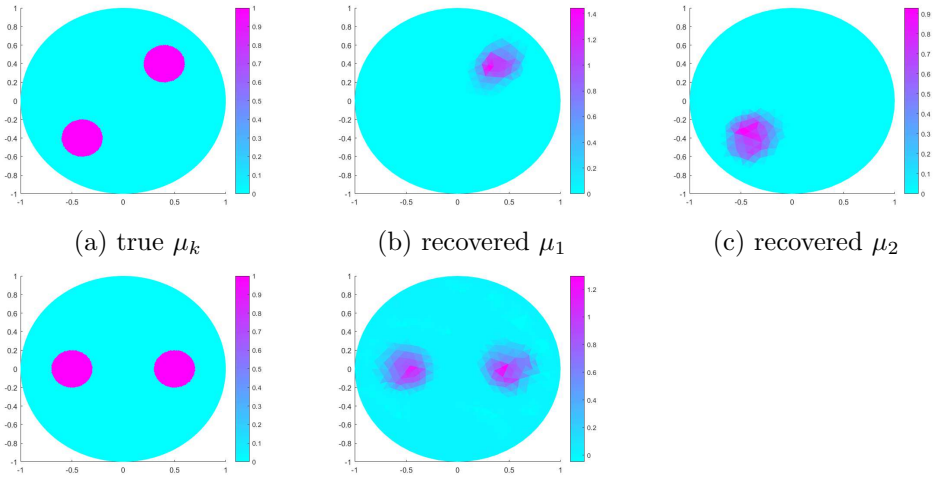

(a) true μ_k (b) recovered μ_1 (c) recovered μ_2

(d) true $\delta d(x)$ (e) recovered $\delta d(x)$

Figure 4.4: Numerical results for Example 4.3: (a) exact μ_1 and μ_2 of two chromophores; (b)-(c) recovered results for two chromophores; (d)-(e) true and recovered $\delta d(x)$.

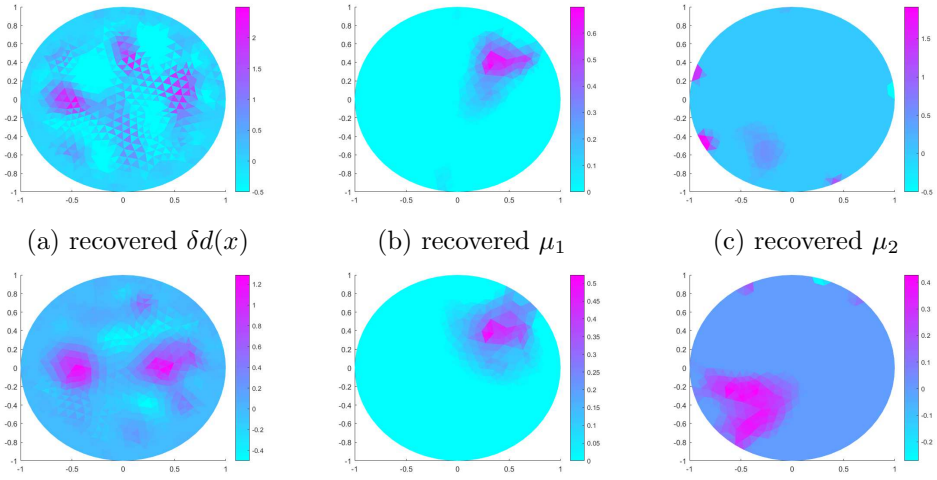

(a) recovered $\delta d(x)$ (b) recovered μ_1 (c) recovered μ_2

(d) recovered $\delta d(x)$ (e) recovered μ_1 (f) recovered μ_2

Figure 4.5: Numerical results for Example 4.4: (a)-(c) the recovered results for case (i) (with 3 wavelengths); (d)-(f): results for case (ii) (with 30 wavelengths).

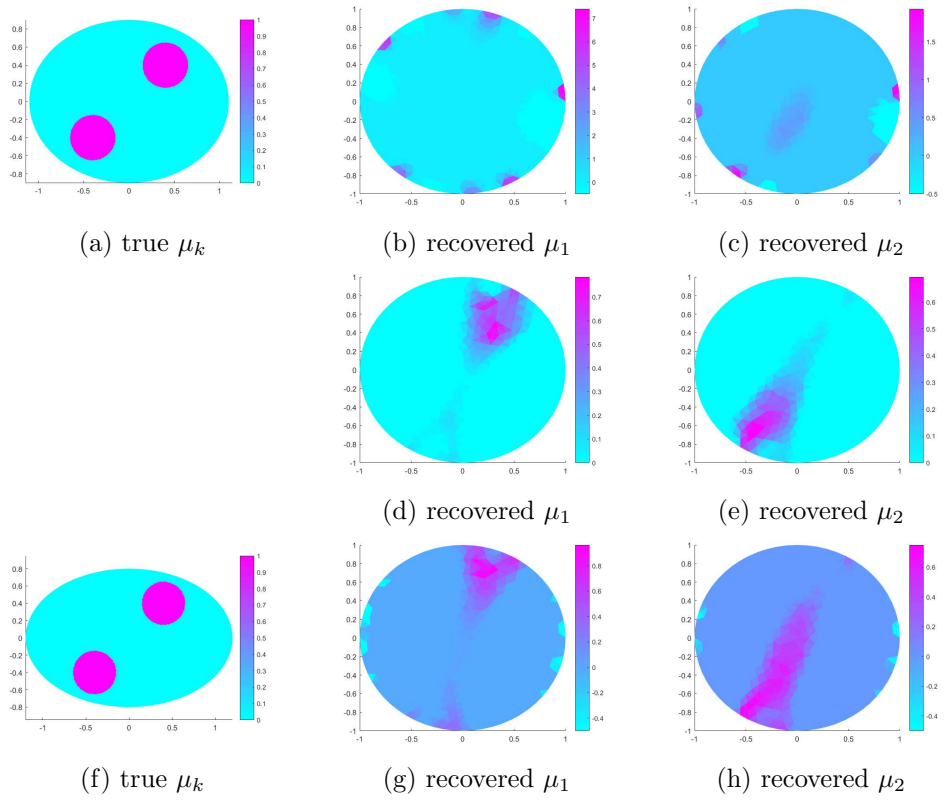

(a) true μ_k (b) recovered μ_1 (c) recovered μ_2

(d) recovered μ_1 (e) recovered μ_2

(f) true μ_k (g) recovered μ_1 (h) recovered μ_2

Figure 4.6: Numerical results for Example 4.5: (a),(f) exact μ_1 and μ_2 of two chromophores in $\widetilde{\Omega}$; (b)-(c) recovered results for two chromophores in Ω for case (i) only using the spectra s_k of the chromophores; (d)-(e) recovered results for two chromophores in Ω for case (i) using the spectra s_k of the chromophores, the spectrum s_0 of the diffusion coefficient and the spectrum $s_*(\lambda) \equiv 1$ of the edge perturbation; (g)-(h) the recovered results for case (ii) using all the spectra s_0, s_k, and s_*.

Example 4.5. *Consider the case of a known diffusion coefficient* $D(\lambda, x) = s_0(\lambda) = 0.2\lambda^{1.5}$*, and two different shape deformations: (i)* $\widetilde{\Omega}$ *is an ellipse with* $a = 1.1$ *and* $b = 0.9$ *and (ii)* $\widetilde{\Omega}$ *is an ellipse with* $a = 1.2$ *and* $b = 0.8$*. Consider two chromophores inside* $\widetilde{\Omega}$*: the wavelength dependence of the chromophore on the top is* $s_1(\lambda) = 0.5(\lambda - 1)$*, and that of the bottom is* $s_2(\lambda) = 0.5(\lambda - 1)^2$*. The measurements are taken at* $Q = 3$ *wavelengths with* $\lambda_1 = 1$*,* $\lambda_2 = 1.5$ *and* $\lambda_3 = 2$*, and the noise level is fixed at* $\eta = 1\%$*.*

The numerical results for Example 4.5 are shown in Figure 4.6. This example illustrates the influence of the deformation scale on the reconstruction. The numerical results show clearly the potential of the multi-wavelength approach: Even using the wrong domain for the inversion step, we can still recover the concentrations of the chromophores (or more precisely the deformed concentrations $\mu_k = \widetilde{\mu}_k \circ F^{-1}$). The numerical results also show even we assume known diffusion coefficient in case (i), we should also use all the spectra s_0, s_k, and s_* to recover the right concentrations of the chromophores (Figures 4.6 (d) and (e)), or the results will be ruined by the shape deformation (Figures 4.6 (b) and (c)).

Example 4.6. *Consider the case of an unknown diffusion coefficient* $D(\lambda, x) = s_0(\lambda)(1 + 0.1\delta d(x)) = 0.2\lambda^{1.5}(1 + 0.25\delta d(x))$*, and the unknown true domain* $\widetilde{\Omega}$ *is an ellipse with* $a = 1.1$ *and* $b = 0.9$*. Consider two chromophores inside the domain* $\widetilde{\Omega}$*: the wavelength dependence of the chromophore on the top is* $s_1(\lambda) = 0.5(\lambda - 1)$*, and that of the bottom is* $s_2(\lambda) = 0.5(\lambda - 1)^2$*. The measurements are taken at* $Q = 3$ *wavelengths with* $\lambda_1 = 1$*,* $\lambda_2 = 1.5$ *and* $\lambda_3 = 2$*, and the noise level is fixed at* $\eta = 1\%$*.*

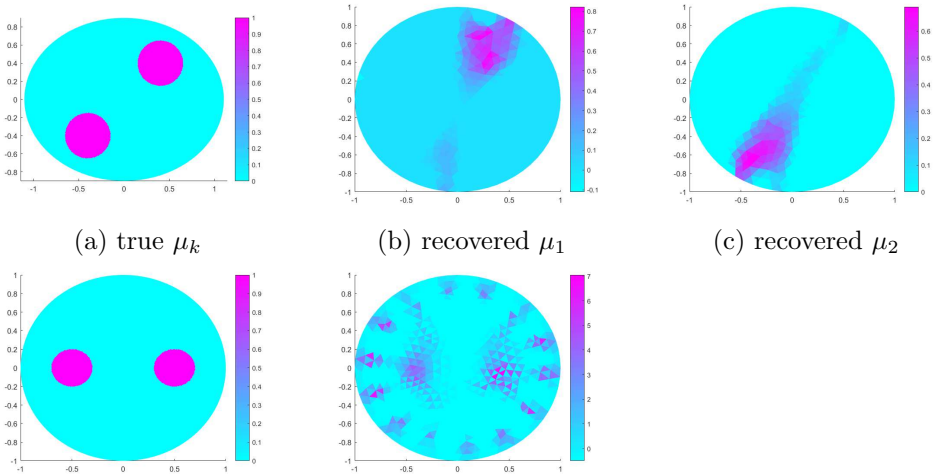

(a) true μ_k (b) recovered μ_1 (c) recovered μ_2

(d) true δd (e) recovered δd

Figure 4.7: Numerical results for Example 4.6: (a),(d): exact μ_1 and μ_2 of two chromophores in $\widetilde{\Omega}$; (b)-(c): recovered results for two chromophores in Ω; (e) the recovered result corresponding to $s_0(\lambda)$.

The numerical results for Example 4.6 are shown in Figure 4.7. It is observed that the two chromophores are recovered well in spite of the imperfectly known boundary, while the diffusion coefficient is totally distorted by domain deformation, and thus it cannot be accurately recovered. The empirical observations on Examples 4.5 and 4.6 concur with the theoretical predictions in Section 3: Proposition 3.1 implies that the domain deformation will be added to the recovered results corresponding to the spectral profile $s_0(\lambda)$ and the diffusion coefficient cannot be recovered due to the domain deformation, but the deformed chromophore concentrations $\mu_k = \widetilde{\mu}_k \circ F^{-1}$ can still be recovered.

5 Conclusion

In this work, we have introduced a novel reconstruction technique for diffuse optical imaging with multi-wavelength data. The approach is based on a linearized model and a group sparsity approach. We have shown that within the linear regime, our reconstruction technique allows recovering the concentration of individual chromophore and the diffusion coefficients, provided that their spectral profiles are known and incoherent. Furthermore, we have demonstrated that the multi-wavelength data can significantly reduce modelling errors associated with an imperfectly known boundary. In fact, it allows recovering well (deformed) concentrations of the chromophores. These findings are fully supported by extensive numerical experiments.

References

[1] G. S. Alberti and H. Ammari. Disjoint sparsity for signal separation and applications to hybrid inverse problems in medical imaging. *Appl. Comput. Harmon. Anal.*, 42(2):319–349, 2017.

[2] G. S. Alberti, H. Ammari, B. Jin, J.-K. Seo, and W. Zhang. The linearized inverse problem in multifrequency electrical impedance tomography. *SIAM J. Imaging Sci.*, 9(4):1525–1551, 2016.

[3] H. Ammari, E. Bossy, V. Jugnon, and H. Kang. Mathematical modeling in photoacoustic imaging of small absorbers. *SIAM Rev.*, 52(4):677–695, 2010.

[4] H. Ammari, E. Bossy, V. Jugnon, and H. Kang. Reconstruction of the optical absorption coefficient of a small absorber from the absorbed energy density. *SIAM J. Appl. Math.*, 71(3):676–693, 2011.

[5] H. Ammari, J. Garnier, L. Giovangigli, W. Jing, and J.-K. Seo. Spectroscopic imaging of a dilute cell suspension. *J. Math. Pures Appl.*, 105(5):603–661, 2016.

[6] H. Ammari, J. Garnier, H. Kang, L. Nguyen, and L. Seppecher. *Multi-Wave Medical Imaging*, volume 2 of *Modelling and Simulation in Medical Imaging*. World Scientific, London, 2017.

[7] H. Ammari and F. Triki. Identification of an inclusion in multifrequency electric impedance tomography. *Comm. Partial Differential Equations*, 42(1):159–177, 2017.

[8] S. R. Arridge. Optical tomography in medical imaging. *Inverse Problems*, 15(2):R41–R93, 1999.

[9] G. Bal and K. Ren. On multi-spectral quantitative photoacoustic tomography in diffusive regime. *Inverse Problems*, 28(2):025010, 13, 2012.

[10] A. N. Bashkatov, E. A. Genina, and V. V. Tuchin. Optical properties of skin, subcutaneous and muscle tissues: a review. *J. Innovat. Opt. Health Sci.*, 04(01):9–38, 2011.

[11] F. Bevilacqua, A. J. Berger, A. E. Cerussi, D. Jakubowski, and B. J. Tromberg. Broadband absorption spectroscopy in turbid media by combined frequency-domain and steady-state methods. *Appl. Optics*, 39(34):6498–6507, 2000.

[12] G. Boverman, E. L. Miller, A. Li, Q. Zhang, T. Chaves, D. H. Brooks, and D. A. Boas. Quantitative spectroscopic diffuse optical tomography of the breast guided by imperfect a priori structural information. *Phys. Med. Biol.*, 50(17):3941–3956, 2005.

[13] A. E. Cerussi, D. B. Jakubowski, N. Shah, F. Bevilacqua, R. M. Lanning, A. J. Berger, D. Hsiang, J. A. Butler, R. F. Holcombe, and B. J. Tromberg. Spectroscopy enhances the information content of optical mammography. *J. Biomed. Optics*, 7(1):60–71, 2002.

[14] A. E. Cerussi, V. W. Tanamai, D. Hsiang, J. Butler, R. S. Mehta, and B. J. Tromberg. Diffuse optical spectroscopic imaging correlates with final pathological response in breast cancer neoadjuvant chemotherapy. *Phil. Trans. Royal Sci.*, 369(1955):4512–4530, 2011.

[15] B. Cox, J. Laufer, S. R. Arridge, and P. C. Beard. Quantitative spectroscopic photoacoustic imaging: a review. *J. Biomed. Opt.*, 17(6):061202, 2012.

[16] B. T. Cox, S. R. Arridge, and P. C. Beard. Estimating chromophore distributions from multiwavelength photoacoustic images. *J. Opt. Soc. Am. A*, 26(2):443–455, 2009.

[17] I. Daubechies, M. Defrise, and C. De Mol. An iterative thresholding algorithm for linear inverse problems with a sparsity constraint. *Comm. Pure Appl. Math.*, 57(11):1413–1457, 2004.

[18] R. Graaff, J. G. Aarnoudse, J. R. Zijp, P. M. A. Sloot, F. F. M. de Mul, J. Greve, and M. H. Koelink. Reduced light-scattering properties for mixtures of spherical particles: a simple approximation derived from Mie calculations. *Appl. Optics*, 31(10):1370–1376, 1992.

[19] F. Hettlich. Fréchet derivatives in inverse obstacle scattering. *Inverse Problems*, 11(2):371–382, 1995.

[20] K. Ito and B. Jin. *Inverse Problems: Tikhonov Theory and Algorithms*. World Scientific, Hackensack, NJ, 2015.

[21] S. L. Jacques. Optical properties of biological tisses: a review. 58(11):R37–R61, 2013.

[22] V. Kolehmainen, M. Lassas, and P. Ola. The inverse conductivity problem with an imperfectly known boundary. *SIAM J. Appl. Math.*, 66(2):365–383, 2005.

[23] J. Laufer, B. Cox, E. Zhang, and P. Beard. Quantitative determination of chromophore concentrations from 2D photoacoustic images using a nonlinear model-based inversion scheme. *Appl. Optics*, 49(8):1219–1233, 2010.

[24] T. O. McBride, B. W. Pogue, E. D. Gerety, S. B. Poplack, U. L. Österberg, and K. D. Paulsen. Spectroscopic diffuse optical tomography for the quantitative assessment of hemoglobin concentration and oxygen saturation in breast tissue. *Appl. Optics*, 38(25):5480–5490, 1999.

[25] A. Pulkkinen, B. T. Cox, S. R. Arridge, J. P. Kaipio, and T. Tarvainen. A Bayesian approach to spectral quantitative photoacoustic tomography. *Inverse Problems*, 30(6):065012, 18, 2014.

[26] D. Razansky, M. Distel, C. Vinegoni, R. Ma, N. Perrimon, R. W. Köster, and V. Ntziachristos. Multispectral opto-acoustic tomography of deep-seated fluorescent proteins in vivo. *Nature Photonics*, 3(7):412–417, 2009.

[27] J. Ripoll and V. Ntziachristos. Quantitative point source photoacoustic inversion formulas for scattering and absorbing media. *Phys. Rev. E*, 71:031912, 9 pp., 2005.

[28] E. M. Sevick, B. Change, J. Leigh, S. Nioka, and M. Maris. Quantitation of time-resolved and frequency-resolved optical spectra for the determination of tissue oxygenation. *Anal. Biochem.*, 195(2):330–351, 1991.

[29] S. Srinivasan, B. W. Pogue, S. Jiang, H. Dehghani, and K. D. Paulsen. Spectrally constrained chromophore and scattering near-infrared tomography provides quantitative and robust reconstruction. *Appl. Optics*, 44(10):1858–1869, 2005.

[30] J. Sylvester. An anisotropic inverse boundary value problem. *Comm. Pure Appl. Math.*, 43(2):201–232, 1990.

[31] Z. Yuan and H. Jiang. Simultaneous recovery of tissue physiological and acoustic properties and the criteria for wavelength selection in multispectral photoacoustic tomography. *Opt. Lett.*, 34(11):1714–1716, 2009.